

Article

Analysis of Simultaneous WPT in Ultra-Low-Power Systems with Multiple Resonating Planar Coils

Jacek Maciej Stankiewicz ^{*}, Adam Steckiewicz  and Agnieszka Choroszucho 

Department of Electrical Engineering, Power Electronics and Power Engineering, Faculty of Electrical Engineering, Białystok University of Technology, Wiejska 45D Str., 15-351 Białystok, Poland; a.steckiewicz@pb.edu.pl (A.S.); a.choroszucho@pb.edu.pl (A.C.)

* Correspondence: j.stankiewicz@doktoranci.pb.edu.pl

Abstract: This paper analyses the conceptual application of a wireless power transfer (WPT) system with multiple resonators supplying outdoor sensors using a mobile charger. The solution is based on the idea of using sensors, located in open space, to monitor environmental parameters. Instead of the typical two-coil WPT with a single charger, energy transfer is realized simultaneously, using a group of identical planar coils as transmitters and receivers connected to the independent power supply circuits of each sensor and microcontroller. By isolating these charged circuits, a higher reliability and powering flexibility of the weather station can be achieved. The concept of the proposed system was discussed, and it was proposed to include the main devices in it. A theoretical analysis was performed considering all mutual couplings and the skin effect; hence, the system is characterized by a matrix equation and sufficient formulae are given. The calculations were verified experimentally for different frequencies, two possible distances between the transmitters and receivers, and equivalent loads. Both the efficiency and load power are compared and discussed, showing that this solution can provide power to ultra-low-power devices, yet the efficiency must still be improved. At the small distance between the transmitting and receiving coils (5 mm), the maximum efficiency value was about 40%, with a load resistance of 10 Ω . By doubling the distance between the coils, the efficiency of the WPT system decreased by three times.

Keywords: wireless power transfer; resonating grids; low-power systems; planar coils



Citation: Stankiewicz, J.M.;

Steckiewicz, A.; Choroszucho, A.

Analysis of Simultaneous WPT in

Ultra-Low-Power Systems with

Multiple Resonating Planar Coils.

Energies **2023**, *16*, 4597. [https://](https://doi.org/10.3390/en16124597)

doi.org/10.3390/en16124597

Academic Editor: Jiafeng Zhou

Received: 15 May 2023

Revised: 1 June 2023

Accepted: 6 June 2023

Published: 8 June 2023



Copyright: © 2023 by the authors.

Licensee MDPI, Basel, Switzerland.

This article is an open access article

distributed under the terms and

conditions of the Creative Commons

Attribution (CC BY) license ([https://](https://creativecommons.org/licenses/by/4.0/)

[creativecommons.org/licenses/by/](https://creativecommons.org/licenses/by/4.0/)

[4.0/](https://creativecommons.org/licenses/by/4.0/)).

1. Introduction

Wireless power transfer (WPT) systems are used in many fields, such as electric vehicle charging [1–4], electric vehicles (PHEVs) [5,6], implantable medical devices (IMDs) [7–9], and consumer electronics [10,11]. WPT technology is used in robotic systems [12], communication sets [13–15], and Internet of Things (IoT) applications [12,13]. WPT technology is divided into two main classes. The first group is radiated far-field WPT [16–18]. The second group is non-radiated near-field WPT. A three-phase charging system was proposed in [6,19]. In [6], it was used to charge an underwater vehicle. In electric vehicles (EV), the coils used have different shapes (circular, planar, square) [20].

Many authors have analysed the shape of these coils and how they are wound. In article [21], an optimized winding model was proposed. In this approach was used a multi-strand Litz wire. This type of wire used allows the skin effect to be reduced, especially at high frequencies. Litz wire is one of the best solutions to reduce the skin effect. Unfortunately, it cannot be used for winding small planar coils. For this reason, in small coils, it is important to know the influence of the skin effect on system efficiency.

In article [22], textile-based coils for a near-field WPT were analysed. The authors researched the production of a textile-based coil taking into account the QI standard. These coils were analysed due to their characteristics. The focus was on the efficiency of the WPT system. In article [23], the authors analysed sewn, laser cut, and printed inductors. The

embroidered coils had diameters of 0.04, 0.05, and 0.06 m. One of the coils was made of a silver-coated yarn. The coil was printed on the carrier fabric. They have shown that this type of coil was not appropriate for the WPT system. The reason was that the resistance of the coil is too high.

The typical topologies are series and parallel combinations. In article [24], the series–parallel mixed topology was analysed. This approach makes the transmission radius larger than the typical serial topology. Transfer efficiency is also greater than the typical parallel topology. In article [25], the authors showed a series–parallel–series topology. This topology allows the power rating to be shifted in the event of significant misalignment. In article [26], the skin effect at high frequency was investigated. The authors showed a plane spiral layout with an air hole. In this approach, they indicated that in order to decrease the skin-effect loss, the thickness of this coil must be the same as the skin depth. The authors of [27,28] proposed various types of array coils, e.g., domino. However, the study was conducted only for the serial configuration, when the series–parallel system had not yet been fully analysed. A pair of coils is used to implement the WPT. Multi-coil technology solutions typically operate at high frequencies. In some cases, power transmission is supported by metamaterial structures [29,30]. In study [31], a project on efficient wireless power distribution systems based on resonant inductive arrays was presented. In this work, the authors showed how to use multi-resonator arrays to charge and power several electrical devices in parallel, with an almost constant transmitted power and using a single power source. The presented wireless power distribution systems improve power transmission efficiency (PTE) in free positioning by up to 30%. The use of arrays to transfer power to freely moving objects was presented in publication [32]. The authors presented an extensible platform for transmitting power to a moving object receiving power from the array. The transmitter consists of two overlapping layers of square planar coils rotated 45 degrees. Each layer consists of four coils to further control the power supply of a small receiving coil. This overlapping star-pattern was automatically stimulated by the power amplifier. By redirecting the current of each small square element in each array with a flower-shaped current, the receiver coil perpendicular to the transmitter plate can obtain power comparable to conventional designs.

In this article, the authors consider the power supply system of the ultra-low-power devices. The group of such receivers includes, e.g., sensors, integrated circuits, low-power communication stations, and wearable electronics. As one of the alternatives of current solutions, a charging method based on many resonators was proposed, where the energy is transferred to the target devices simultaneously and independently. This approach makes it possible to increase the reliability of the charger and makes possible the operation of receiving devices by using its own WPT system, battery, and electric separation of individual circuits from each receiver. Thus, potential damage or abnormal operation (including short-circuits and overvoltages) of the resonators, rectifier, battery, or connecting cables of one of the receivers will not significantly affect the functionality of the others. However, a multi-coil system with more than one load requires prior analysis of its electrical parameters, i.e., mainly power and efficiency, before being used in practice. Hence, an uncomplicated circuit model (but at the same time one considering the most important phenomena) is needed for research and design purposes. Section 2 presents the idea of creating such a multi-element circuit. An example of this could be an autonomous set of sensors recharged by a mobile energy source. The electrical model of this system was characterized taking into account a series of couplings representing mutual coupling through the magnetic field. A laboratory stand for the preliminary, experimental verification of the theoretical research is also described. Section 3, in addition to the characterization of the exemplary WPT device, contains a comparison of the results of theoretical calculations and measurements performed on the test stand. The influence of the dependence of efficiency and power on the frequency and the equivalent load resistance was presented. Section 4 is devoted to a summary of the work and the most important conclusions drawn from the conducted research.

2. Materials and Methods

2.1. Multi-Coil Wireless Charging System

Multiple planar coils can be used simultaneously to transfer energy to one or multiple loads. The parallel connection of the inductors and the subsequent operation of the inductive power transfer device (IPT) reduces the potential resistive losses from one larger coil or a series of connected coils, i.e., in configurations with an equivalent resistance higher than in a parallel topology. For example, such a topology was previously presented in [33,34], where the transmitting and receiving surfaces, consisting of periodically arranged planar inductors, were mainly analysed using numerical models. Possible applications were associated with the simultaneous power supply of beacons and sensors placed in walls/roofs or with electric vehicles (e.g., forklifts) operating in a limited area, under which a WPT system was installed for continuous energy transfer to the vehicle. The prospective implementation is also wireless rechargeable sensor networks (WRSN) with unmanned aerial vehicles (UAV) as energy sources. These networks have raised the interest recently [35,36], since they make it possible to create a wirelessly connected group of sensors deployed in any area where widespread UAVs provide charging capability.

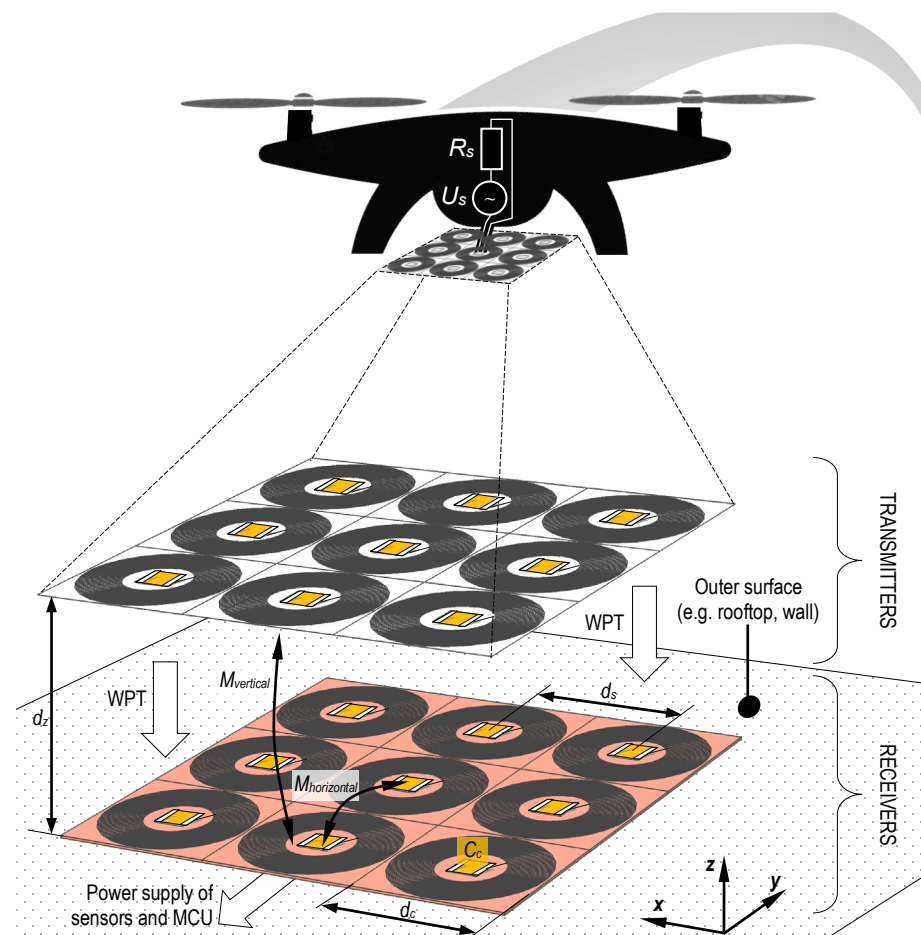


Figure 1. An exemplary realization of the concept of charging multiple low-power devices—a drone (energy source) with transmitting coils approaches the surface (e.g., a rooftop) with mounted receivers to charge the batteries connected to sensors and other electronic modules.

In the previous works, a simplified infinite grid was considered, and some parameters (mutual inductances) were identified numerically. Here, the finite grid was examined, and no numerical models were used during the analysis. The considered situation (Figure 1) concerns the case in which the UAV is equipped with a battery pack, an inverter, and a matching network, which (from the point of view of the electrical circuit) can be interpreted

as a voltage source U_s with an internal resistance R_s . At the bottom of the UAV, a set of coils has been installed—they will act as energy sources in the WPT. While on the small landing pad, placed at any outer surface, identical coils are secured and connected to a group of sensors. In the simplest of assumptions, these sensors will require a battery, a microcontroller unit (MCU) to control the operation of the system, and a wireless communication module (TR), as shown in Figure 2. We can distinguish an example set of probes to measure environmental properties such as temperature, humidity, air pressure, air quality, CO₂, magnetic field, and sun sensors. Furthermore, a TR device with an antenna and an MCU power supply is required. In this scenario, each module has its own transmitting (Tx) and receiving (Rx) resonators: the rectifier and battery. Hence, a failure or disruption of any module (despite the TR and MCU) will not affect the operation of other devices. For example, damage due to the overvoltage of the Rx resonator and the rectifier of the humidity sensor will not affect the others, because other modules have individual receivers.

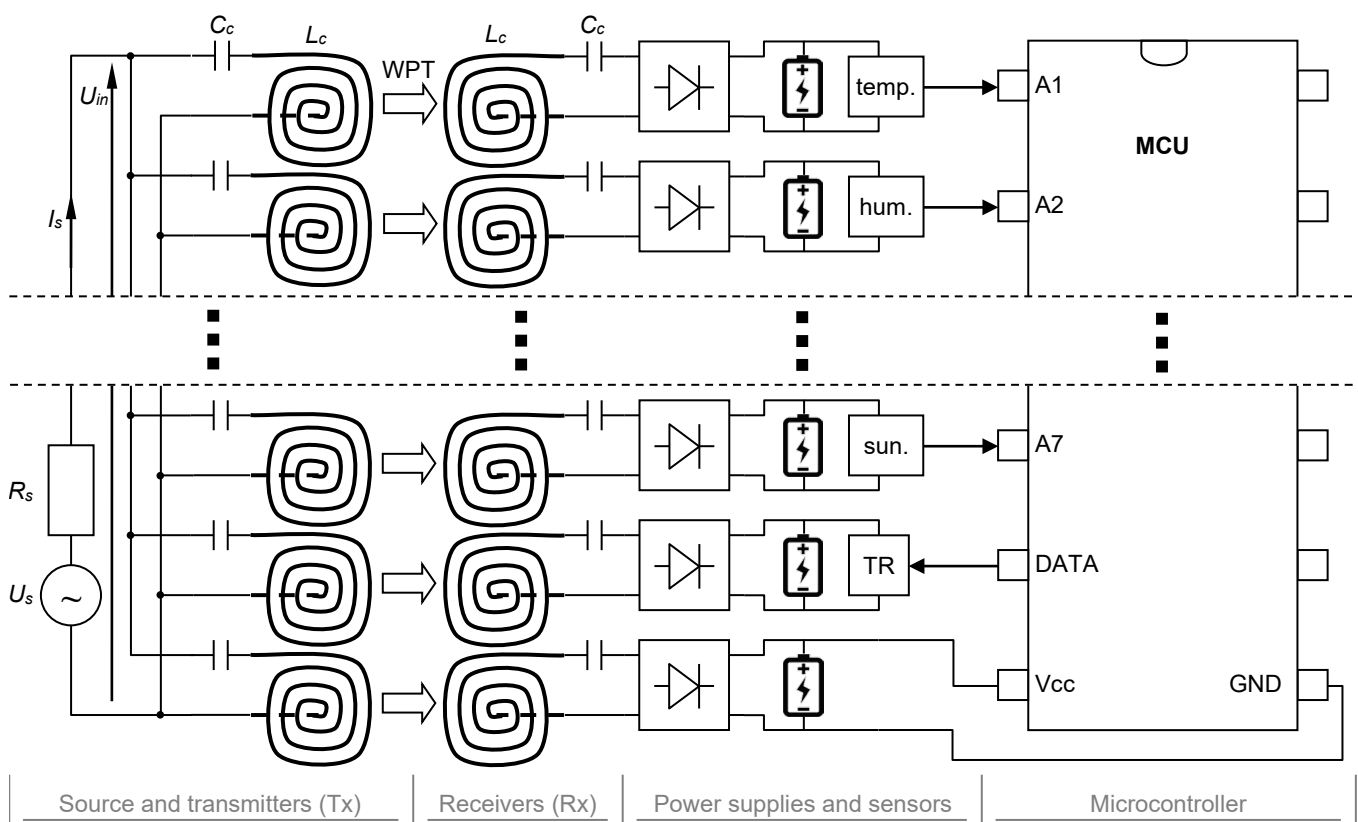


Figure 2. The schematic of an exemplary measurement system of sensors (temperature, humidity, sunlight, etc.) with a communication module (TR) and a microcontroller (MCU), powered by a mobile energy source (U_s , R_s) using a wireless power transfer (WPT) with resonant coils (L_c , C_c).

In this case, nine devices (7 sensors + TR + MCU) were considered; therefore, nine Tx/Rx resonators were used. To “standardize” the problem, all resonators were identical and made as circular planar coils, characterized by self-inductance (L_c), with a series-connected lumped capacitor (C_c). Additionally, any DC load in an AC circuit can be modelled as an equivalent resistance (R), representing the resulting combination of the rectifier, battery, and functional device. The receivers are isolated from each other; meanwhile, the transmitters are connected in parallel.

However, according to Figures 2 and 3, with a marked voltage drop in U_{in} at the input terminals, each Tx coil can be connected to a different voltage source, for example, a separate battery pack with an inverter. This will ensure galvanic separation between the transmitters and the possibility of individual U_{in} control. In the presented variant, the transmitters are connected to a single source. The purpose of this was to reproduce

the ability to use the UAV's main battery pack with only one inverter. It also simplified the analysis of the system at the preliminary research stage, helping to identify its basic features and limitations and the relevance of the simulation model.

2.2. Equivalent Electrical Circuit

The WPT power supply system is based on two square surfaces consisting of nine resonators (Figure 3) with outer size d_c , a wound with a wire of diameter d_w and insulation thickness d_i , where the number of turns was n_t . Numbers 1–9 were assigned to the Tx circuits, while numbers 10–18 were assigned to the Rx circuits. Due to the parallel connection of the Tx resonators, an equal voltage drop (U_{in}) was found at the input terminals, while the Rx coils directly powered the loads R_9 – R_{18} . The WPT was made by magnetically coupling the Tx and Rx sides. However, the energy transfer occurred not only between two vertically facing coils (Figure 1), but also horizontally and diagonally, i.e., between any one coil and the other seventeen.

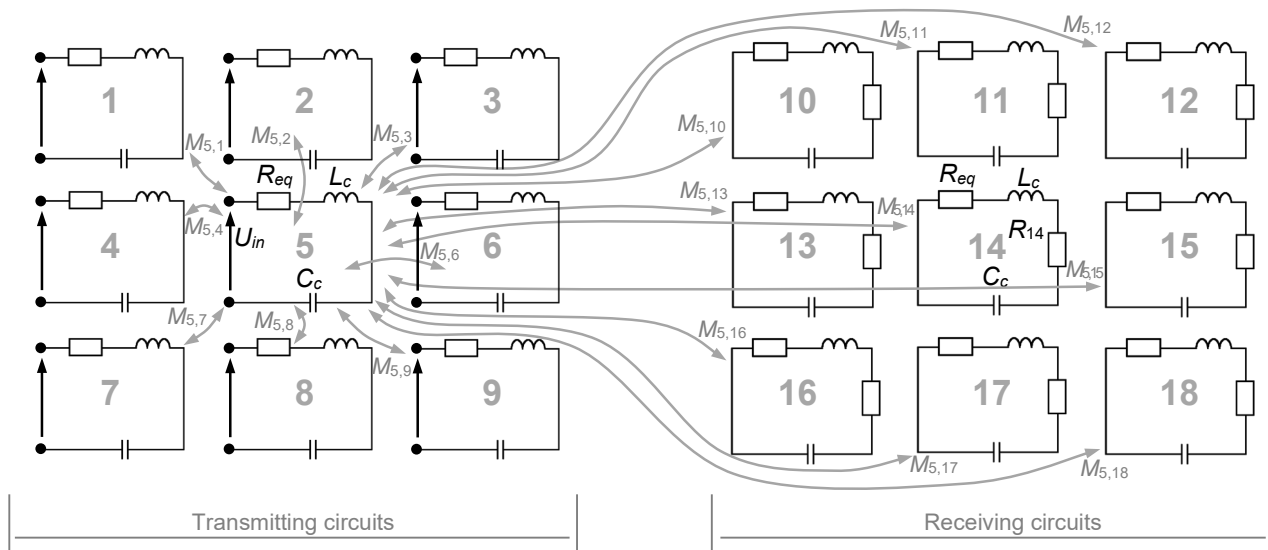


Figure 3. The electrical circuits of the transmitting and receiving surfaces with magnetic couplings: each a -th coil is magnetically coupled with the other b -th coil by the mutual inductance $M_{a,b}$ (like the example inductor no. 5).

The mutual inductance ($M_{a,b}$) of an arbitrary coil and any planar resonator (a and b were the numbers of these coils, respectively) can be found using formula [37]:

$$M_{a,b} = \frac{\mu_0 s^2}{4\pi} \int_{\Phi_1}^{\Phi_0} \int_{\Phi_1}^{\Phi_0} \frac{(1 + \varphi_1 \varphi_2) \cos(\varphi_2 - \varphi_1) - (\varphi_2 - \varphi_1) \sin(\varphi_2 - \varphi_1)}{\sqrt{d_z^2 + (d_x + s\varphi_2 \cos \varphi_2 - s\varphi_1 \cos \varphi_1)^2 + (d_y + s\varphi_2 \sin \varphi_2 - s\varphi_1 \sin \varphi_1)^2}} d\varphi_1 d\varphi_2, \quad (1)$$

where s is the screw pitch, $s = (d_w + d_i)/(2\pi)$ in [m]; Φ_1 is the starting angle of the spiral, $\Phi_1 = [d_c/2 - (d_w + d_i)n_t]/s$; Φ_0 is the ending angle of the spiral, $\Phi_0 = d_c/2s$; φ_1, φ_2 is the angles of rotation along the edge of the spiral. Additionally, d_z is the vertical distance (between coil a and b) in [m]; d_x, d_y are the horizontal distances (between the a and b coil) along the x and y axes in [m] (Figure 1). One may see that the entire set of mutual inductances is responsible for transferring power from the source (U_s, R_s) to the loads (R_{10} – R_{18}) and as a result generates redundant transmission paths, even in the case of a failure of the Tx coil. Equation (1) can be solved numerically by using summation instead of a double integral and dividing the angles into discrete steps:

$$M_{a,b} = \frac{\mu_0 s^2 \Phi_N^2}{4\pi} \sum_{n_2=\Phi_s}^{N+\Phi_s} \sum_{n_1=\Phi_s}^{N+\Phi_s} \frac{(1 + n_2 n_1 \Phi_N^2) \cos(n_2 \Phi_N - n_1 \Phi_N) - (n_2 \Phi_N - n_1 \Phi_N) \sin(n_2 \Phi_N - n_1 \Phi_N)}{\sqrt{d_z^2 + (d_x + s n_2 \Phi_N \cos n_2 \Phi_N - s n_1 \Phi_N \cos n_1 \Phi_N)^2 + (d_y + s n_2 \Phi_N \sin n_2 \Phi_N - s n_1 \Phi_N \sin n_1 \Phi_N)^2}}, \quad (2)$$

where Φ_N is the discrete step, $\Phi_N = (\Phi_o - \Phi_i)/N$; Φ_s is the starting step, $\Phi_s = \Phi_i/\Phi_N$; N is the number of subintervals, $N > 2(d_c/2s)$. With a higher number of N , the accuracy of Equation (2) tends to be the exact solution of Equation (1).

From Equation (2), the self-inductance (L_c) of the coil can be determined, which can be interpreted as the mutual inductance of the considered inductor and itself. Hence, to identify L_c , substitute $d_z = d_x = d_y = 0$ and simplify the final formula as shown below:

$$L_c = \frac{\mu_0 s \Phi_N}{4\pi} \sum_{n_2=\Phi_s}^{N+\Phi_s} \sum_{n_1=\Phi_s}^{N+\Phi_s} \frac{(1 + n_2 n_1 \Phi_N^2) \cos(n_2 \Phi_N - n_1 \Phi_N) - \Phi_N (n_2 - n_1) \sin(n_2 \Phi_N - n_1 \Phi_N)}{\sqrt{n_1^2 + n_2^2 - 2n_1 n_2 \cos(n_1 \Phi_N - n_2 \Phi_N)}}. \tag{3}$$

For identical resonators, L_c needs to be calculated only once, unlike $M_{a,b}$, which needs to be identified for all pairs of coils in the system. When the self-inductance is known, the capacitance (C_c) of the compensating capacitor, at an assumed desired frequency of f_c , can be found as:

$$C_c = \frac{1}{4\pi^2 f_c^2 L_c}. \tag{4}$$

In practical situations, the compensating capacitor has its own internal resistance. To easily model this series resistance (ESR) of C_c , the equation from [38] was used:

$$R_{ESR} = \frac{DF}{2\pi f C_c}, \tag{5}$$

where DF is the dissipation factor; f is the AC current frequency in [Hz].

Then, the coil resistance (R_c) is calculated. Firstly, the length (l) of an Archimedean spiral needs to be found. Despite the exact formulae expressing this quantity, a rough estimate of the length was made by multiplying the average coil circumference by the number of turns (n_t):

$$l = 2\pi \underbrace{\frac{\overbrace{\frac{d_c}{2}}^{\text{outer radius}} + \frac{\overbrace{\frac{d_c}{2} - n_t(d_w + d_i)}^{\text{inner radius}}}{2}}_{\text{mean radius}}} n_t = \pi n_t [d_c - n_t(d_w + d_i)]. \tag{6}$$

An unknown resistance is given by the formula for the finite length (determined by Equation (6)) of a straight conductor, known as:

$$R_c = \frac{l}{\sigma a_{eff}} = \frac{\pi n_t [d_c - n_t(d_w + d_i)]}{\sigma a_{eff}}, \tag{7}$$

where σ is the electrical conductivity of the conductor (wire) in [S/m]; a_{eff} is the effective cross-section of the conductor (wire) in [m²]. In the high-frequency electromagnetic field, there is a skin effect; therefore, the effective cross-section was taken from [39]:

$$a_{eff} = \pi \delta_{eff} (d_w - \delta_{eff}), \tag{8}$$

where δ_{eff} is the effective skin depth in [m]. The parameter δ_{eff} is expressed by the equation:

$$\delta_{eff} = (\pi f \sigma \mu_0)^{-1/2} \left[1 - \exp\left(\frac{-d_w}{2(\pi f \sigma \mu_0)^{-1/2}}\right) \right]. \tag{9}$$

Finally, the equivalent resistance of the resonator (Figure 3) was:

$$R_{eq} = k_R (R_{ESR} + R_c), \tag{10}$$

where k_R is the coefficient responsible for the undesirable increase in resistance in real applications. Due to the appearance of contact and solder resistance, impedance of the connecting wires, temperature rise in the presence of a positive temperature coefficient, capacitor leakage resistance, other parasitic resistances in the system (e.g., solder pads and printed copper paths), etc., the resulting equivalent resistance $R_{eq} > (R_{ESR} + R_c)$.

When the lumped parameters are found using Equations (2)–(5) and Equations (7) and (10) at the desired frequency f_c , then the currents in each resonator can be calculated. The simplest system of equations to be solved is obtained from Kirchhoff’s voltage law:

$$\begin{cases} ZI_a + j\omega \sum_{b=1}^B M_{a,b} I_b = U_{in}, & \forall b, a \leq \frac{B}{2}, a \neq b \\ ZI_a + j\omega \sum_{b=1}^B M_{a,b} I_b + R_a = 0, & \forall b, a > \frac{B}{2}, a \neq b \end{cases} \quad (11)$$

where Z is the resonator impedance, $Z = R_{eq} + j\omega L_c + (j\omega C_c)^{-1}$ in $[\Omega]$; I_a is the current in a -th resonator in [A], B is the number of all resonators. The matrix equation $\mathbf{A} \cdot \mathbf{I} = \mathbf{U}$, where \mathbf{A} is the impedance matrix, can be derived from Equation (11) for the general case with B resonators and different loads:

$$\begin{bmatrix} Z & j\omega M_{1,2} & \cdots & j\omega M_{1,B/2} & j\omega M_{1,B/2+1} & j\omega M_{1,B/2+2} & \cdots & j\omega M_{1,B} \\ \vdots & \vdots & \ddots & \vdots & \vdots & \vdots & \ddots & \vdots \\ j\omega M_{B/2,1} & j\omega M_{B/2,2} & \cdots & Z & j\omega M_{B/2,B/2+1} & j\omega M_{B/2,B/2+2} & \cdots & j\omega M_{B/2,B} \\ j\omega M_{B/2+1,1} & j\omega M_{B/2+1,2} & \cdots & j\omega M_{B/2+1,B/2} & Z + R_{B/2+1} & j\omega M_{B/2+1,B/2+2} & \cdots & j\omega M_{B/2+1,B} \\ \vdots & \vdots & \ddots & \vdots & \vdots & \vdots & \ddots & \vdots \\ j\omega M_{B,1} & j\omega M_{B,2} & \cdots & j\omega M_{B,B/2} & j\omega M_{B,B/2+1} & j\omega M_{B,B/2+2} & \cdots & Z + R_B \end{bmatrix} \cdot \begin{bmatrix} I_1 \\ \vdots \\ I_{B/2} \\ I_{B/2+1} \\ \vdots \\ I_B \end{bmatrix} = \begin{bmatrix} U_{in} \\ \vdots \\ U_{in} \\ 0 \\ \vdots \\ 0 \end{bmatrix} \quad (12)$$

where ω is the angular frequency, $\omega = 2\pi f$ in [rad/s]. Since, in most possible cases, B would be less than several dozen, the unknown vector of currents ($\mathbf{I} = \mathbf{A}^{-1} \cdot \mathbf{U}$) can be calculated with no effort. Equation (12) allows for a multi-parameter analysis of the designed system, e.g., for various coils, compensation capacitors, loads, and faults (short-circuits, disconnections, etc.) in the WPT device. The efficiency can be estimated as

$$\eta = \frac{S_{out}}{S_{in}} 100\% = \frac{\sum_{n=B/2+1}^B \frac{U_n^2}{R_n}}{U_{in} I_s} 100\% = \frac{\sum_{n=B/2+1}^B R_n |I_n|^2}{U_{in} \left| \sum_{n=1}^{B/2} I_n \right|} 100\%, \quad (13)$$

where S_{out} is the output apparent power (sum of real power of loads) in [VA]; S_{in} is the input apparent power (sum of power on input terminals) in [VA]; U_n is the RMS voltage of n -th load in [V]; R_n is the resistance of the n -th load in $[\Omega]$; I_n is the complex current of the n -th resonator in [A]; I_s is the RMS value of the source current in [A]. One must be aware that the resonance state can be obtained only at a specific frequency, as complex input power (S_{in}) only has its real part, while in practice, the resonance point may differ slightly for each resonator, causing reactive power to be present in the WPT circuit, but still allowing energy to be transferred to the loads. This situation is also worth considering using Equation (12).

2.3. Experimental Stand

The model in Section 2.2 was verified using the experimental stand. The circular planar coils were wound and connected to capacitors. A procedure that was adopted relied on creating $B = 18$ identical coils, measuring their self-inductances and matching individual capacitors to each of them in order to obtain one desired resonant frequency f_c , according to Equation (4). As energy receivers ($R_{B/2+1} \div R_B$) variable resistors were used, helping to adjust their resistance and test their influence on the WPT efficiency.

Two surfaces were made, each with 9 resonators (Figure 4), mounted on a gripper located on a horizontal slide to adjust the distance d_z between the surfaces. During the measurements, the *Rigol DG4062* signal generator ($U_s = 7$ V, $R_s = 50$ Ω) was used as the source, while the voltages and currents were measured by probes connected to the *Rigol DS2072* oscilloscope. The measured quantities are U_{in} (the RMS value of the input voltage), I_s (the RMS value of the source current) and $U_{B/2+1} \div U_B$ (the RMS value of the load voltages). Based on these values, the powers and efficiency were calculated using Equation (13). All parameters used during the experiments and theoretical calculations are presented in Table 1.

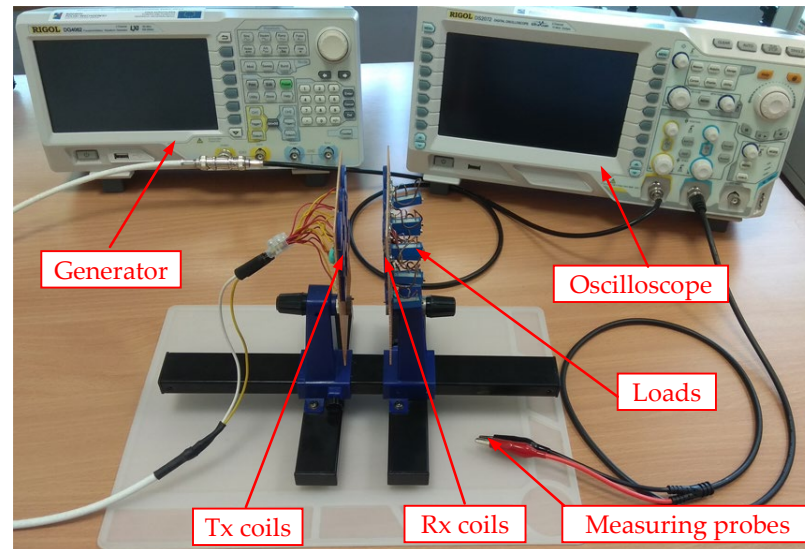


Figure 4. Experimental stand with transmitting and receiving coils, mounted on an adjustable holder, connected to a signal generator and an oscilloscope.

Table 1. Parameters of the WPT system.

Number of turns	n_t	30
Wire diameter	d_w	200 μm
Insulation thickness	d_i	5 μm
Coil diameter	d_c	20 mm
Separation between coils	d_s	25 mm
Distances between transmitters and receivers	d_z	5 mm
Design frequency	f_c	10 mm
Electrical conductivity	σ	500 kHz
Dissipation factor	DF	5.6×10^7 S/m
Resistance increase coefficient	k_R	0.05
		1.25

The circuit model from Equation (12) was solved for the above-mentioned parameters in the *Matlab R2022b* software and compared with the experimental results. Mutual inductances ($M_{a,b}$) were also determined by the numerical calculation of Equation (2) and inductance of coils using Equation (3) for $N = 1000$ subintervals. The numerical considerations required one self-inductance (L_c), but in the general case $B(B - 1)/2 = 153$, mutual inductances had to be identified. However, due to the internal and external symmetry of the transmitting and receiving surfaces, only 11 mutual inductances were estimated, which greatly reduced the calculation time.

3. Results and Discussion

3.1. Analyzed Cases

The experimental and analytical results are compared and presented in Section 3.3 (power transfer efficiency) and Section 3.4 (transferred power), at the distances $d_z = 5$ mm and $d_z = 10$ mm. The influence of the load resistance on the power and efficiency of the WPT system was tested at the design frequency and the results are presented in Section 3.3.1. Variable resistors connected to each receiving coil were used as energy receivers, which allowed us to adjust the load resistance and study their influence on the efficiency of the WPT system. The influence of the frequency of the source voltage, over a frequency range of 100 kHz to 1000 kHz with a load resistance of $R = 50 \Omega$ connected to each receiving coil, on the parameters of the WPT system was also tested, and the results are presented in Section 3.3.2. The results from the experimental stand are presented as solid green lines (marked as *Measurements* in the legend). The results from the circuit model are shown as solid red lines (marked as *Calculations* in the legend). Finally, the output power is discussed in Section 3.4, where the variability and maximum achievable powers are presented.

3.2. Measured Parameters

Table 2 presents the measured parameters of the coils and capacitors used in the experiment (L_c , R_c and C_c). The capacitances were matched to each coil individually to obtain a resonant frequency of $f_c = 500$ kHz. Since each coil had a different self-inductance, the capacitors also varied. Even so, the relative standard deviation was less than 10%, with 8.16% for inductance, 2.34% for resistance, and 8.25% for capacitance.

Table 2. Measured lumped parameters of coils and compensation capacitors.

No.	L_c (μH)	R_c ($\text{m}\Omega$)	C_c (nF)
1	16.12	862	6.29
2	14.55	855	6.96
3	14.72	912	6.88
4	13.11	850	7.73
5	15.60	871	6.49
6	13.25	854	7.65
7	17.11	864	5.92
8	14.58	863	6.95
9	13.80	831	7.34
10	14.78	839	6.86
11	15.16	860	6.68
12	14.40	858	7.04
13	15.76	875	6.43
14	15.45	869	6.56
15	14.98	909	6.76
16	16.60	879	6.10
17	16.82	872	6.02
18	13.06	858	7.76
Average	14.99	866	6.80

It was important to properly tune the capacitors, because, taking into account Equation (4) and only the average values of the measured quantities (Table 2), we obtained a resonant frequency of 498.43 kHz, which is lower than the desired f_c . Meanwhile, the lumped parameters calculated for the simulation, using the *Matlab* software, were $L_c = 13.84 \mu\text{H}$, $R_c = 753 \text{ m}\Omega$, $C_c = 7.32 \text{ nF}$, perfectly produced $f_c = 500$ kHz. In real life applications, tuning and/or extremely precise coil fabrication will be required. Furthermore, the relative difference between the measured (average value) and the calculated inductance was -7.67% ; for the resistance, the relative difference was -13.05% ; and for the capacitance, the relative difference was 7.65% . The higher values of the measured

inductance and resistance resulted from the fact that the coils used in the experiment were slightly longer, which were, not ideally, tightly wound and with extra elongations (“pins”) so that they could be connected to the printed circuit board.

Therefore, existing mismatches and the structure of the simulation model will result in possible limitations or divergences between the measurements and calculations. The equivalent circuit with the presented formulas for inductance and resistance will not be able to model the ferrite material often used in experimental research and applications. The presence of parasitic conductors (copper pads, casing, metal joining, etc.) clearly affects the WPT, while in the circuit model, these negative effects can only be partially addressed by the k_R factor. As a result, the lumped parameters, resonant frequency, efficiency, and power may differ from the measured ones by up to several percent (as was the case regarding the capacitance and resistance mentioned above).

3.3. Power Transfer Efficiency

3.3.1. The Influence of the Load Resistance

The influence of the load resistance on the efficiency of the WPT system at the resonant frequency was analysed. This part compares the results of the calculations and measurements of the WPT system at the distances of $d_z = 5$ mm (Figure 5a) and $d_z = 10$ mm (Figure 5b).

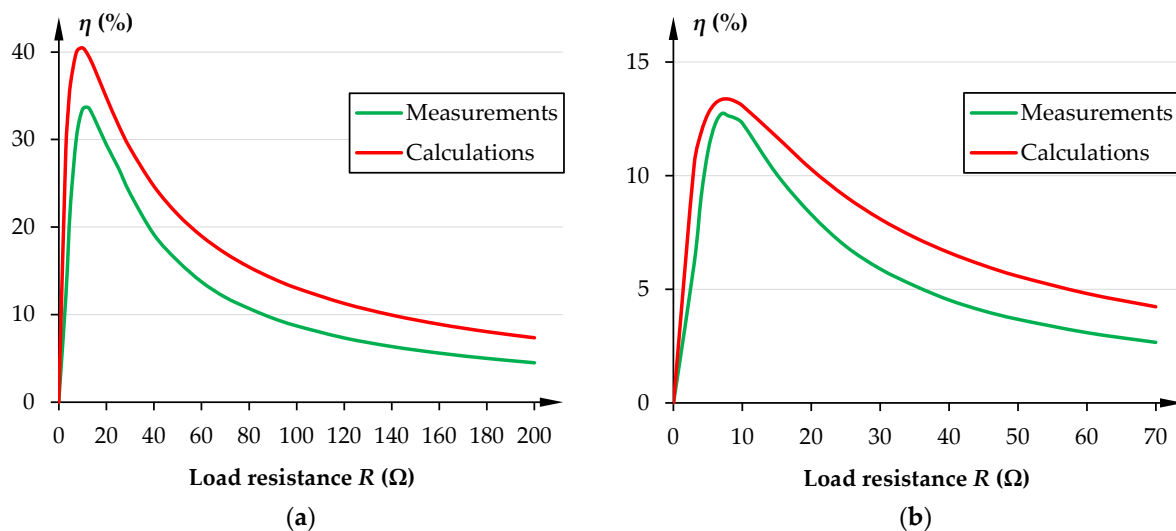


Figure 5. Power transfer efficiency for various loads at the distances: (a) $d_z = 5$ mm and (b) $d_z = 10$ mm.

On the experimental stand, it was additionally measured that the resonant frequency was at a frequency of 576 kHz at the distance $d_z = 5$ mm, and at a frequency of 550 kHz at the distance $d_z = 10$ mm, while the designed resonant frequency was 500 kHz. In both cases analysed, the shape of the characteristics obtained from measurements and calculations was maintained. The power transfer efficiency of the WPT system increased as the load resistance increased, and then began to decrease after reaching the maximum value. At the distance $d_z = 5$ mm, the maximum efficiency value obtained by the measurements was 33.65% with a load resistance of 12.5 Ω , while the maximum efficiency value obtained by the calculations was 40.47% with a load resistance of 10 Ω (Figure 5a). The greatest difference in the WPT system efficiency results obtained by the measurements and calculations (about 15%) occurs at low load resistance values and decreases with increasing load resistance (it does not exceed 3%). At the distance $d_z = 10$ mm, the maximum efficiency value obtained by the measurements was 12.73% with a load resistance of 7 Ω , while the maximum efficiency value obtained by the calculations was 13.36% with a load resistance of 8 Ω (Figure 5b). The maximum efficiency of the WPT system was thus reduced by about three times. The greatest difference in the WPT system efficiency results obtained from measurements and calculations (about 4%) occurs at low load resistance values, while the smallest difference (less than 0.5%) occurs at the load resistance for which maximum efficiency was obtained.

3.3.2. The Influence of the Frequency at the Constant Load

The influence of the frequency of the source voltage over a frequency range of 100 kHz to 1000 kHz with a load resistance of 50Ω , on the efficiency of the WPT system, was analysed. This part compares the results of calculations and measurements of the WPT system, at the distances $d_z = 5$ mm (Figure 6a) and $d_z = 10$ mm (Figure 6b).

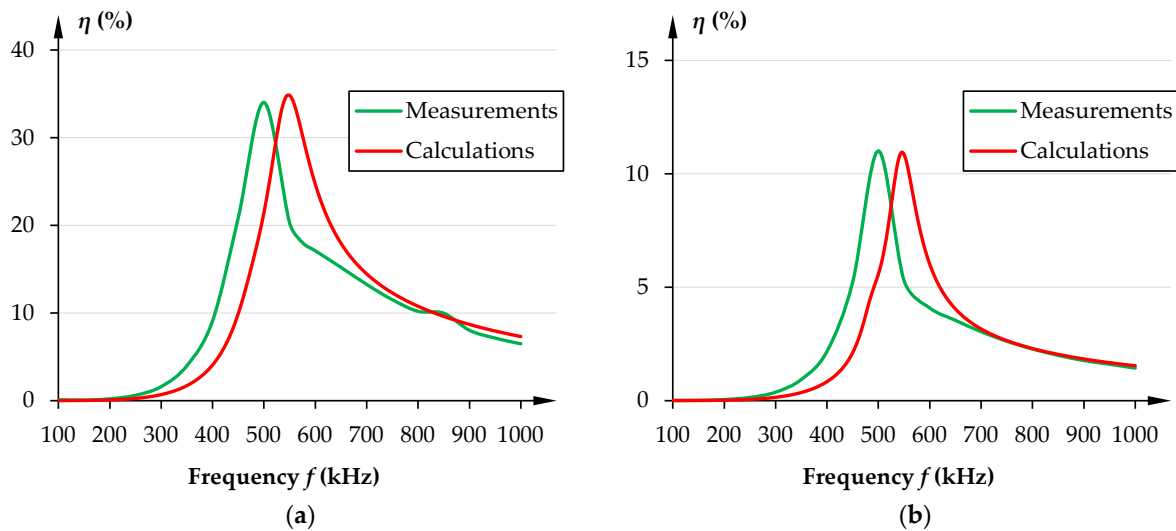


Figure 6. Power transfer efficiency for different frequencies at the distances: (a) $d_z = 5$ mm and (b) $d_z = 10$ mm.

In both cases analysed, the shape of the characteristics obtained from the measurements and calculations was maintained. At the distance $d_z = 5$ mm, the maximum efficiency value obtained from the measurements and calculations was similar and amounted to about 35% (Figure 6a) for measurements at the frequency of 500 kHz, but for calculations at the frequency of 550 kHz. The greatest difference in efficiency results for the WPT system was over the frequency range of 400 kHz–600 kHz. At the distance $d_z = 10$ mm, the maximum efficiency value obtained from the measurements and calculations was identical and amounted to about 11% (Figure 6b) for measurements at the frequency of 500 kHz, but for calculations at the frequency of 550 kHz. The greatest difference in efficiency results for the WPT system was over the frequency range of 400 kHz–600 kHz.

3.4. Transferred Power

The power transferred to the loads was in fact an active power, due to the resistive nature of the energy receivers, and it varied depending on the load resistance and frequency. Furthermore, the multi-coil and resulting multi-coupling nature of the WPT system complicated the theoretical analysis, where analytically finding the optimal load resistance (maximizing the output power) became much more difficult. In order to determine the variation of the output power (S_{out}) with the load and frequency, the maximum achievable value of S_{out} and the adjustment of the load resistance, the characteristics (Figures 7 and 8) from the measurements and calculations are presented in this section.

The dependence of the total load power on the load resistance (Figure 7) had almost the same shape as the power transfer efficiency (Figure 5). On the other hand, the peak value of the transmitted power, i.e., $\max(S_{out})$ at $d_z = 5$ mm, was different for both the experimental and the circuit model, with $R_{opt,meas.} = 10.06 \Omega$ and $R_{opt,calc.} = 12.49 \Omega$, respectively (relative difference 24.16%). Meanwhile, the $\max(S_{out})$ at $d_z = 10$ mm was achieved for $R_{opt,meas.} = 8.01 \Omega$ and $R_{opt,calc.} = 7 \Omega$ (relative difference: -12.61%). It is clear that the distance between the Tx and Rx coils affects the value of the matching resistance—the greater the distance, the lower the load resistance. Despite the indicated differences, the-

oretical calculations accurately predicted this relationship; hence, they can be helpful in determining the power and optimal load resistance at the stage of system analysis/design.

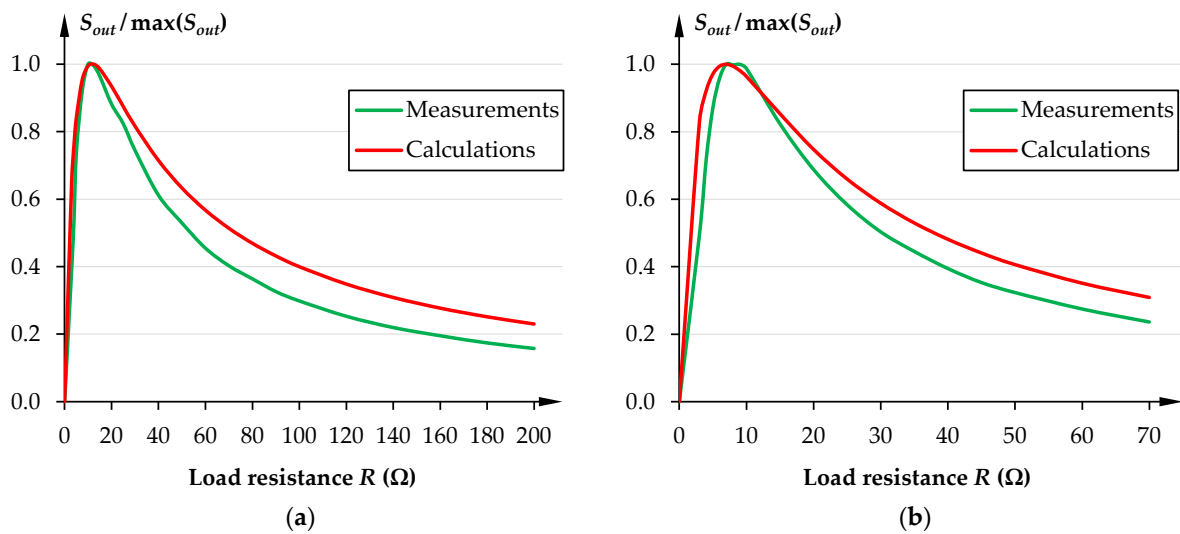


Figure 7. Relative load power for various loads at the distances: (a) $d_z = 5$ mm and (b) $d_z = 10$ mm.

Since the wireless power supply operates most efficiently at its resonant frequency, the characteristics (Figure 8) can show the true resonance point (f_c') at the highest achieved power, $S_{out}/\max(S_{out}) = 1$, in this case for a constant load resistance of $R = 50$ Ω . With no doubt, the resonant frequency found by the measurements ($f_c' = 500$ kHz) is noticeably lower than found by the calculations ($f_c' = 550$ kHz). Interestingly, the values of these frequencies were not affected by the distance d_z . The resonant frequency shift in the circuit model is due to the mutual coupling between an arbitrary coil and the other coils (excluding the coil directly in front where the main energy transfer occurred). The simplest explanation is to overestimate the mutual inductances in the model using Equation (2), comparing them to the much lower values produced in reality. Nevertheless, the measured and calculated output power showed the same dependence on the frequency and “width” of the peaks and their changes—in Figure 8a, the bandwidths were $BW_{meas.} = 78$ kHz and $BW_{calc.} = 54$ kHz, while in Figure 8b, the bandwidths were $BW_{meas.} = 67$ kHz and $BW_{calc.} = 36$ kHz. The output power varies more dynamically than the power transfer efficiency (Figure 6), which should be kept in mind when considering multi-load and multi-band WPT.

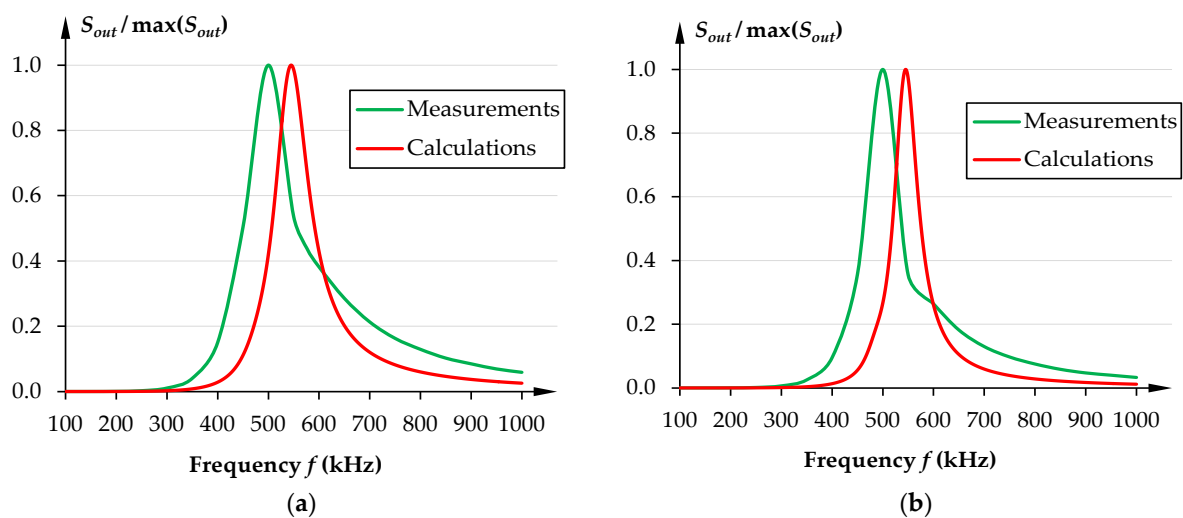


Figure 8. Relative load power for different frequencies at the distances: (a) $d_z = 5$ mm and (b) $d_z = 10$ mm.

Finally, the maximum output powers are discussed. In Table 3, the $\max(S_{out})$ values are presented; however, they have been recalculated for a more practical voltage supply, e.g., $U_{in} = 9$ V, where U_{in} is construed as the voltage at the input ports of the transmitting coils (Figures 2 and 3).

Table 3. Maximum achievable load power values, $\max(S_{out})$, recalculated for $U_{in} = 9$ V.

Varying Parameter	$d_z = 5$ mm	$d_z = 10$ mm	Change
Load resistance, with a measured resonance at 500 kHz	28.05 VA	12.11 VA	−56.83%
Frequency, with a theoretical resonance at 550 kHz	42.31 VA	18.46 VA	−56.37%

Under these conditions, the power ranged from a dozen to several dozen volt-amperes, which would be sufficient to power small electronic devices, even with fast charging. The highest maximum powers were obtained for the calculated resonant point ($f_c' = 550$ kHz) with a load of $R = 50 \Omega$, theoretically reaching 42.31 VA and 18.46 VA at $d_z = 5$ mm and $d_z = 10$ mm, respectively. The output power was reduced by approximately 56% after doubling the distance. However, for the designed resonant frequency ($f_c = 500$ kHz), the powers for $R = 50 \Omega$ were equal to 18 VA and 4.98 VA, i.e., they were several times lower. Hence, it is crucial to analyse the system using a model or prototype to first find the actual resonance point and then determine the optimal resistance there. On the other hand, keeping to only the designed frequency and based on Figure 7, it can be concluded that the optimal resistances are $R = 12.49 \Omega$ and $R = 8.01 \Omega$, which, at $f_c = 500$ kHz, provide the maximum achievable powers of 28.05 VA and 12.11 VA (Table 3).

3.5. The Effect of Distance on the System Performance

The variability of the distance (d_z) between the transmitter and the receiver and its influence on the efficiency and load power were also studied. Because the UAV may land imperfectly on the landing pad, its deformation or undesirable objects on the surface (e.g., dirt or dust) causing “vertical misalignment”, the actual distance (d_z) may increase. On the other hand, due to the appearance of a casing of Tx and Rx arrays, d_z cannot be less than a certain minimum value. For example, fabricated coils had a carcass thickness of 2 mm; hence, the minimum distance was $\min(d_z) = 4$ mm. This lower limit is marked on the figures with a grey dashed line at $d_z/d_c = 0.2$. The analysis was carried out for six loads (5, 10, 12.5, 25, 50, and 100 Ω) and two operating frequencies: 500 kHz (the design frequency) and 550 kHz (the resonance point).

The outcome was as expected: efficiency decreased with increasing distance, but for $d_z/d_c > 0.5$, there was a sharp decrease in all cases, where, at $d_z/d_c = 1$, the values approached zero (Figure 9). For $d_z > \min(d_z)$, the highest efficiencies were found for the previously identified optimal resistances, i.e., 10 and 12.5 Ω . Interestingly, near $d_z/d_c = 0.2$, and then for $d_z/d_c > 0.3$, the efficiency for $R = 5 \Omega$ was higher than for $R \geq 25 \Omega$. However, below $\min(d_z)$, higher resistances ($R \geq 25 \Omega$) gave higher efficiency. Furthermore, for $f = 550$ kHz, the all-present increase in power transfer efficiency (η) was noticed (Figure 9b). To conclude, in a real application, it would be better to use an operating frequency as close as possible to the real resonance point, and relatively small load resistances to maximize the η . In the fabricated system, the load can even vary from a few to several ohms, and still, at any practically useful distance, a similar efficiency will be achieved.

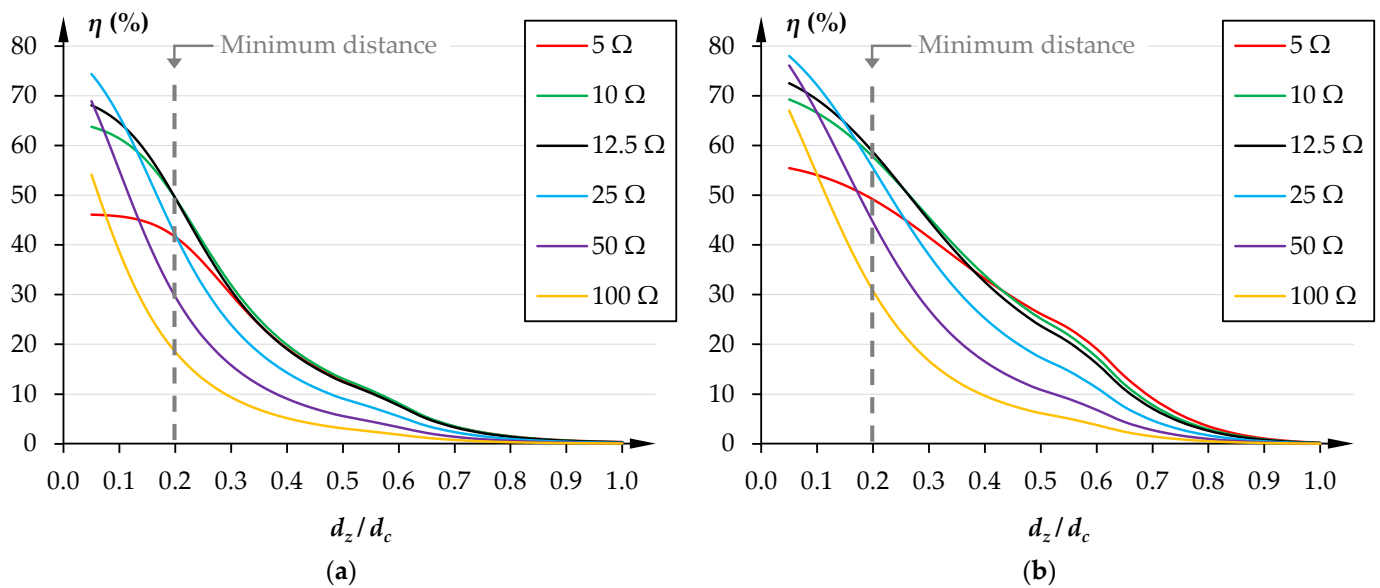


Figure 9. Power transfer efficiency at different distances and loads at operating frequencies: (a) $f = 500$ kHz and (b) $f = 550$ kHz.

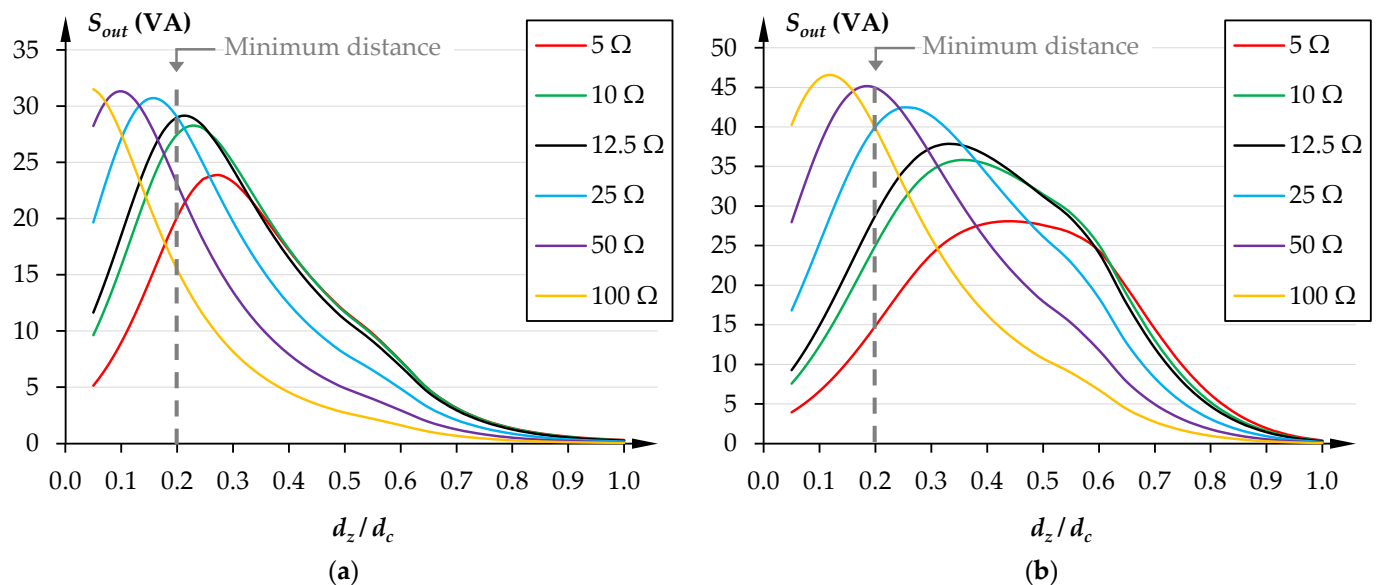


Figure 10. Load power at different distances and loads at operating frequencies: (a) $f = 500$ kHz and (b) $f = 550$ kHz.

The load power also varied with distance; at that time, the function was not monotone (Figure 10). Maximum values were found at certain specified d_z/d_c ; however, for $R \geq 50 \Omega$, the peaks appeared below $\min(d_z)$. For $d_z/d_c > 0.3$, only smaller loads were able to provide more power. If both the efficiency and output power must be maximized, the load must be noticeably lower than 50Ω . This opens the possibility of using the proposed solution for effective fast charging; since resistance is a scale factor between voltage and current, a low-resistance energy receiver means a load powered by a higher current (crucial in fast charging systems).

In Table 4, the highest identified efficiencies are presented with the corresponding parameters. Once again, the previous conclusions can be seen, in which the highest efficiency was obtained using low-resistance loads, and their powers were comparable ($27.59 \div 34.39$ VA), being sufficient to power a group of low-power electronic devices. The

only problematic case was $f = 500$ kHz and $d_z/d_c = 0.5$ ($d_z = 10$ mm), because the overall efficiency was unacceptable ($\eta_{\max} = 13.08\%$, $S_{out} = 11.67$ VA).

Table 4. Maximum efficiency (η_{\max}) at specified distances and parameters at which they were obtained (for $U_{in} = 9$ V).

f (kHz)	d_z/d_c	d_z (mm)	R (Ω)	η_{\max} (%)	S_{out} (VA)
500	0.20	4	12.5	49.43	28.99
	0.25	5	10	40.47	27.91
	0.50	10	10	13.08	11.67
550	0.20	4	12.5	58.69	28.83
	0.25	5	12.5	51.94	34.39
	0.50	10	5	26.13	27.59

The last comparison can be made based on Table 5, where the efficiency of the system at three distances is presented. Let us choose the load resistances that provide the best balance between efficiency and load power. At the shortest distance ($d_z/d_c = 0.2$), the best balance was for $R = 12.5 \Omega$ (500 kHz), where η was the highest value and S_{out} was the second highest value, or for $R = 25 \Omega$ (550 kHz), where η was the third highest and S_{out} was again the second highest result. As distance increased ($d_z/d_c = 0.25$), the resistances decreased: the best cases were $R = 10 \Omega$ (500 kHz) and $R = 12.5 \Omega$ (550 kHz), having the highest η and the second- (or third-) highest S_{out} . Finally, at $d_z/d_c = 0.5$, only $R = 10 \Omega$ maximized the efficiency and provided nearly the highest output power. Hence, when the load is characterized by a relatively low equivalent resistance, the system can achieve both one of the highest possible efficiencies and one of the highest possible output powers.

Table 5. Comparison of the efficiency and output power for different loads, distances, and frequencies.

d_z/d_c	d_z (mm)	R (Ω)	500 kHz		550 kHz	
			η (%)	S_{out} (VA)	η (%)	S_{out} (VA)
0.2	4	5	41.62	20.13	49.16	14.86
		10	49.43	27.49	57.72	25.01
		12.5	49.43	28.99	58.69	28.83
		25	42.07	29.02	55.47	40.03
		50	29.60	23.08	44.58	44.94
		100	18.48	15.49	30.79	39.84
0.25	5	5	36.47	23.59	45.62	19.70
		10	40.47	27.91	51.83	30.79
		12.5	39.57	28.05	51.94	34.39
		25	31.72	24.54	46.36	42.47
		50	21.45	17.96	34.83	42.31
		100	13.02	11.21	22.59	32.66
0.5	10	5	12.71	11.76	26.13	27.59
		10	13.08	11.67	25.17	31.49
		12.5	12.43	11.03	23.72	31.24
		25	9.08	7.99	17.34	26.14
		50	5.57	4.98	10.86	18.46
		100	3.10	2.75	6.15	10.74

4. Conclusions

This paper focuses on the analysis of the application of a wireless power transfer system with multiple resonators. The concept of the proposed system is discussed, and a theoretical analysis was carried out. The calculations were verified using experiments carried out with different frequencies, two possible distances between the transmitters and receivers, and the equivalent loads. Efficiency and load power at two distances between coils are compared and discussed.

In the cases analysed, the shape of the characteristics obtained using measurements and calculations was maintained. The maximum power transfer efficiency obtained using the measurements was almost seven percent lower than that obtained using the calculations. By doubling the distance between the coils, the efficiency of the WPT system decreased by three times. The distance between the transmitting and receiving coils affected the value of the matching resistance, i.e., the greater the distance, the lower the load resistance. Despite the indicated differences, theoretical calculations appropriately predicted this dependency; hence, they can be helpful in identifying the powers and optimum load resistance at the stage of system analysis. The highest maximum powers were found for the calculated resonance point, so it is crucial to analyse the system using a model or a prototype to firstly find the actual resonance point and then identify the optimal resistance there. Such a solution could provide power supply to ultra-low-power devices, but the efficiency still needs to be improved.

The authors plan to focus further research on the analysis of other coil shapes (e.g., pentagonal and hexagonal). The authors are also considering the possibility of using metamaterials in the proposed WPT systems to increase the efficiency of the system.

Author Contributions: The paper was written by J.M.S., A.S. and A.C. The methodology was developed by J.M.S. and A.S. The results presented in this paper were performed by J.M.S. and A.S. The analysis was performed by J.M.S. and A.S. The review, editing, and improvements to the content were made by J.M.S. and A.C. Funding acquisition was done by J.M.S. All authors have read and agreed to the published version of the manuscript.

Funding: The printing of the article was financed from the **ZIREG project—Integrated Program of the Bialystok University of Technology for Regional Development**, contract no. POWR.03.05.00-00-ZR22/18. Project co-financed by the European Union from the European Social Fund under the Knowledge Education Development Operational Program 2014–2020.

Data Availability Statement: Not applicable.

Conflicts of Interest: The authors declare no conflict of interest.

References

1. Sun, L.; Ma, D.; Tang, H. A review of recent trends in wireless power transfer technology and its applications in electric vehicle wireless charging. *Renew. Sustain. Energy Rev.* **2018**, *91*, 490–503. [[CrossRef](#)]
2. Luo, Z.; Wei, X. Analysis of Square and Circular Planar Spiral Coils in Wireless Power Transfer System for Electric Vehicles. *IEEE Trans. Ind. Electron.* **2018**, *65*, 331–341. [[CrossRef](#)]
3. Batra, T.; Schaltz, E.; Ahn, S. Effect of ferrite addition above the base ferrite on the coupling factor of wireless power transfer for vehicle applications. *J. Appl. Phys.* **2015**, *117*, 17D517. [[CrossRef](#)]
4. Inoue, K.; Kusaka, K.; Itoh, J.I. Reduction in radiation noise level for inductive power transfer systems using spread spectrum techniques. *IEEE Trans. Power Electron.* **2018**, *33*, 3076–3085. [[CrossRef](#)]
5. Tang, S.C.; Lun, T.L.T.; Guo, Z.; Kwok, K.W.; McDannold, N.J. Intermediate range wireless power transfer with segmented coil transmitters for implantable heart pumps. *IEEE Trans. Power Electron.* **2017**, *32*, 3844–3857. [[CrossRef](#)]
6. Kan, T.; Mai, R.; Mercier, P.P.; Mi, C.C. Design and analysis of a three-phase wireless charging system for lightweight autonomous underwater vehicles. *IEEE Trans. Power Electron.* **2017**, *33*, 6622–6632. [[CrossRef](#)]
7. Nithyanandam, V.; Sampath, V. Approach-Based Analysis on Wireless Power Transmission for Bio-Implantable Devices. *Appl. Sci.* **2023**, *13*, 415. [[CrossRef](#)]
8. Li, X.; Zhang, H.; Peng, F.; Li, Y.; Yang, T.; Wang, B.; Fang, D. A wireless magnetic resonance energy transfer system for micro implantable medical sensors. *Sensors* **2012**, *12*, 10292–10308. [[CrossRef](#)]
9. Fitzpatrick, D.C. *Implantable Electronic Medical Devices*; Academic Press: San Diego, CA, USA, 2014; pp. 7–35.
10. Kang, S.H.; Choi, J.H.; Jung, C.W. Magnetic resonance wireless power transfer using three-coil system with single planar receiver for laptop applications. *IEEE Trans. Consum. Electron.* **2015**, *61*, 160–166.
11. Barman, S.D.; Reza, A.W.; Kumar, N.; Karim, M.E.; Munir, A.B. Wireless powering by magnetic resonant coupling: Recent trends in wireless power transfer system and its applications. *Renew. Sustain. Energy Rev.* **2015**, *51*, 1525–1552. [[CrossRef](#)]
12. Sugino, M.; Kondo, H.; Takeda, S. Linear motion type transfer robot using the wireless power transfer system. In Proceedings of the 2016 International Symposium on Antennas and Propagation (ISAP), Okinawa, Japan, 24–28 October 2016; pp. 508–509.
13. Wu, Q.; Tao, M.; Kwan Ng, D.W.; Chen, W.; Schober, R. Energy-efficient resource allocation for wireless powered communication networks. *IEEE Trans. Wirel. Commun.* **2016**, *15*, 2312–2327. [[CrossRef](#)]

14. Zouaoui, S.; Dghais, W.; Melicio, R.; Belgacem, H. Omnidirectional WPT and Data Communication for Electric Air Vehicles: Feasibility Study. *Energies* **2020**, *13*, 6480. [[CrossRef](#)]
15. Chorozucho, A.; Butryło, B. Local attenuation of electromagnetic field generated by wireless communication system inside the building. *Przegląd Elektrotechniczny* **2011**, *87*, 123–127.
16. Khang, S.T.; Lee, D.J.; Hwang, I.J.; Yeo, T.D.; Yu, J.W. Microwave power transfer with optimal number of rectenna arrays for midrange applications. *IEEE Antennas Wirel. Propag. Lett.* **2018**, *17*, 155–159. [[CrossRef](#)]
17. De Santi, C.; Meneghini, M.; Caria, A.; Dogmus, E.; Zegaoui, M.; Medjdoub, F.; Kalinic, B.; Cesca, T.; Zaroni, E. GaN-based laser wireless power transfer system. *Materials* **2018**, *11*, 153. [[CrossRef](#)]
18. Li, Q.; Deng, Z.; Zhang, K.; Wang, B. Precise attitude control of multitrotary-joint solar-power satellite. *J. Guid. Control Dyn.* **2018**, *41*, 1435–1442. [[CrossRef](#)]
19. Yu, L.; Wu, L.; Zhu, Y.; Cao, X.; Zhang, G.; Xiang, S. Wireless Charging Concave Coil Design for UAVs. *Electronics* **2022**, *11*, 1962. [[CrossRef](#)]
20. Rayan, B.A.; Subramaniam, U.; Balamurugan, S. Wireless Power Transfer in Electric Vehicles: A Review on Compensation Topologies, Coil Structures, and Safety Aspects. *Energies* **2023**, *16*, 3084. [[CrossRef](#)]
21. Abou Houran, M.; Yang, X.; Chen, W. Free Angular-Positioning Wireless Power Transfer Using a Spherical Joint. *Energies* **2018**, *11*, 3488. [[CrossRef](#)]
22. Micus, S.; Padani, L.; Haupt, M.; Gresser, G.T. Textile-Based Coils for Inductive Wireless Power Transmission. *Appl. Sci.* **2021**, *11*, 4309. [[CrossRef](#)]
23. Sun, D.; Chen, M.; Podilchak, S.; Georgiadis, A.; Abdullahi, Q.S.; Joshi, R.; Yasin, S.; Rooney, J.; Rooney, J. Investigating flexible textile-based coils for wireless charging wearable electronics. *J. Ind. Text.* **2020**, *50*, 333–345. [[CrossRef](#)]
24. Chen, L.; Liu, S.; Zhou, Y.C.; Cui, T.J. An optimizable circuit structure for high-efficiency wireless power transfer. *IEEE Trans. Ind. Electron.* **2013**, *60*, 339–349. [[CrossRef](#)]
25. Villa, J.L.; Sallan, J.; Sanz Osorio, J.F.; Llombart, A. High-misalignment tolerant compensation topology for icpt systems. *IEEE Trans. Ind. Electron.* **2012**, *59*, 945–951. [[CrossRef](#)]
26. Lee, S.-H.; Lorenz, R.D. Development and validation of model for 95%-efficiency 220-w wireless power transfer over a 30-cm air gap. *IEEE Trans. Ind. Appl.* **2011**, *47*, 2495–2504. [[CrossRef](#)]
27. Zhong, W.; Lee, C.K.; Hui, S.Y.R. General analysis on the use of Tesla's resonators in domino forms for wireless power transfer. *IEEE Trans. Ind. Electron.* **2013**, *60*, 261–270. [[CrossRef](#)]
28. Alberto, J.; Reggiani, U.; Sandrolini, L.; Albuquerque, H. Fast calculation and analysis of the equivalent impedance of a wireless power transfer system using an array of magnetically coupled resonators. *Prog. Electromagn. Res. B* **2018**, *80*, 101–112. [[CrossRef](#)]
29. Xun, J.-H.; Mu, Y.; Zhang, K.; Liu, H.; Li, L. The Efficiency Improvement of Multiple Receivers in Wireless Power Transmission by Integrating Metasurfaces. *Materials* **2022**, *15*, 6943. [[CrossRef](#)]
30. Steckiewicz, A. Homogenization of the vertically stacked medium frequency magnetic metamaterials with multi-turn resonators. *Sci. Rep.* **2022**, *12*, 20333. [[CrossRef](#)]
31. Mirbozorgi, S.A.; Maghsoudloo, E.; Bahrami, H.; Sawan, M.; Gosselin, B.A. Multi-resonator arrays for smart wireless power distribution: Comparison with experimental assessment. *IET Power Electron.* **2021**, *13*, 4189–4193. [[CrossRef](#)]
32. Pahlavan, S.; Shooshtari, M.; Jafarabadi Ashtiani, S. Star-Shaped Coils in the Transmitter Array for Receiver Rotation Tolerance in Free-Moving Wireless Power Transfer Applications. *Energies* **2022**, *15*, 8643. [[CrossRef](#)]
33. Stankiewicz, J.M.; Chorozucho, A. Efficiency of the Wireless Power Transfer System with Planar Coils in the Periodic and Aperiodic Systems. *Energies* **2022**, *15*, 115. [[CrossRef](#)]
34. Stankiewicz, J.M. Analysis of the Influence of the Skin Effect on the Efficiency and Power of the Receiver in the Periodic WPT System. *Energies* **2023**, *16*, 2009. [[CrossRef](#)]
35. Shu, Y.; Yousefi, H.; Cheng, P.; Chen, J.; Gu, Y.; He, T.; Shin, K.G. Near-Optimal Velocity Control for Mobile Charging in Wireless Rechargeable Sensor Networks. *IEEE Trans. Mob. Comput.* **2016**, *15*, 1699–1713. [[CrossRef](#)]
36. Chen, T.-S.; Chen, J.-J.; Gao, X.-Y.; Chen, T.-C. Mobile Charging Strategy for Wireless Rechargeable Sensor Networks. *Sensors* **2022**, *22*, 359. [[CrossRef](#)]
37. Liu, S.; Su, J.; Lai, J. Accurate Expressions of Mutual Inductance and Their Calculation of Archimedean Spiral Coils. *Energies* **2019**, *12*, 2017. [[CrossRef](#)]
38. Torki, J.; Joubert, C.; Sari, A. Electrolytic capacitor: Properties and operation. *J. Energy Storage* **2023**, *58*, 106330. [[CrossRef](#)]
39. Knight, D.W. Practical Continuous Functions for the Internal Impedance of Solid Cylindrical Conductors. G3YNH. 2016. Available online: <https://g3ynh.info/zdocs/comps/Zint.pdf> (accessed on 1 May 2023).

Disclaimer/Publisher's Note: The statements, opinions and data contained in all publications are solely those of the individual author(s) and contributor(s) and not of MDPI and/or the editor(s). MDPI and/or the editor(s) disclaim responsibility for any injury to people or property resulting from any ideas, methods, instructions or products referred to in the content.